13th International Conference on
Structural Health Monitoring of Intelligent Infrastructure
DOI: 10.3217/978-3-99161-057-1-149

Towards structural health monitoring of clay-printed structures

Jasper Vollmert [0009-0001-6245-912X], Patricia Peralta [0000-0002-1923-7142], Adel Alatassi [0009-0006-2862-5530], Alexander Chmelnizkij, and Kay Smarsly [0000-0001-7228-3503]
Institute of Digital and Autonomous Construction, School of Civil and Environmental Engineering, Hamburg University of Technology, Blohmstraße 15, 21079 Hamburg, Germany
Email: jasper.vollmert@tuhh.de, patricia.peralta.abadia@tuhh.de, adel.alatassi@tuhh.de, alexander.chmelnizkij@tuhh.de, kay.smarsly@tuhh.de

ABSTRACT: Structural health monitoring (SHM) is a well-established practice to ensure safety and reliability of civil structures. With the increasing demand for environmentally responsible construction practices and the need to reduce the carbon footprint of construction projects, sustainable materials, such as clay, are gaining attention. Clay-printed structures introduce a novel domain to SHM that requires adaptations of established SHM strategies. Research on SHM strategies devised for clay-printed structures remains scarce, leaving a critical gap in understanding the long-term performance of clay-printed structures. Serving as a foundation for developing SHM strategies for clay-printed structures, this paper proposes a methodology to experimentally determine the structural behavior of clay-printed structures, including buckling, shrinkage, and load-bearing capacity, while identifying key factors critical for developing SHM strategies. The methodology proposed in this study incorporates condition assessment, constraint definition, design optimization, prototyping, and SHM strategy definition. The methodology is implemented for a wall component to experimentally determine shrinkage. Based on the structural behavior of the wall component, an SHM strategy is proposed that essentially consists of selecting appropriate SHM techniques, defining sensor placement, and establishing decision-making criteria. The results demonstrate the feasibility of constructing structurally stable clay-printed structures and provide key insights into SHM strategies for clay-printed structures, advancing sustainable construction practices.

KEY WORDS: Additive manufacturing; clay printing, structural health monitoring, sustainable construction.

1 INTRODUCTION

Digital fabrication techniques, particularly 3D printing (3DP), have witnessed increasing adoption across various industries in recent years [1]. The construction sector has been adopting 3DP technologies over the past two decades, scaling up 3DP processes to meet the demands of large-scale building projects and enabling environmentally responsible construction practices. The trend towards using 3DP in construction has encouraged research on automating construction processes, owing to well-developed digital-based construction methods as well as research on 3DP materials, such as concrete and clay [2].

Data on the long-term performance of 3D-printed structures and on the internal state of 3D-printed materials is essential for understanding relationships between 3DP processes, materials and geometries [3]. By monitoring structural aspects, such as buckling, shrinkage, and load-bearing capacity, the long-term performance of 3D-printed structures may be determined and assessed. Consequently, structural health monitoring (SHM) may facilitate data recording and analysis to monitor the long-term performance of 3DP structures. However, SHM methodologies tailored to 3D-printed structures, particularly clay-printed structures, barely exist [4].

Generally, embedded sensors may enhance monitoring of structural and material behavior of clay-printed structures. In 3DP applications, embedded sensors have been largely deployed for concrete printing and in a lesser extent for clay printing [5]. Since sensing in concrete printing is more mature compared to sensing in clay printing [6], synergies between concrete and clay printing may be exploited to monitor structural parameters (e.g., strain and deformation) and material parameters (e.g., temperature and moisture content) of clay-printed structures. For example, lead zirconate titanate piezoelectric sensors, utilizing electro-mechanical impedance techniques, provide real-time insights into the stability of stacked layers and help assess potential structural weaknesses during printing [7]. Strain gauges and linear variable displacement transducers are used to evaluate buckling characteristics in complex 3D-printed walls under compressive loading [8]. Similarly, fiber Bragg grating sensors embedded in clay capture internal strain changes and allow measuring critical parameters, such as temperature and pressure variations [9]. However, current sensing techniques lack a systematic approach, hindering the development of SHM methodologies for clay-printed structures.

Latest studies in clay printing have primarily relied on visual inspection of in-situ tests, with limited emphasis on systematic evaluation techniques [10]. Moreover, sensor placement in clay-printed structures has been determined by trial-and-error testing rather than structured investigation. Hence, research on SHM methodologies specifically tailored to clay-printed structures remains limited. Thus, by deploying a generalized experimental testing methodology, SHM strategies may be defined to assess the behavior and improve the understanding of long-term performance of clay-printed structures. For example, shrinkage, which may cause structural instabilities [11], could be assessed by monitoring temperature and moisture content during the drying process to minimize desiccation cracks.

In this paper, a methodology for defining an SHM strategy for clay-printed structures is proposed. The methodology considers structural and material behavior, comprising

DOI: 10.3217/978-3-99161-057-1-149

condition assessment, constraint definition, design optimization, prototyping, and, finally, SHM strategy definition.

The reminder of this paper is structured as follows. First, an overview of the proposed methodology is presented. The methodology is implemented by experimental testing to derive an SHM strategy. Next, the effectiveness of the SHM strategy is validated by embedding sensors to monitor moisture content. Finally, the paper concludes with a summary and a concluding synthesis of the key findings.

2 METHODOLOGY

The methodology is devised to propose a scientifically sound SHM strategy and it consists of five phases, condition assessment, constraint definition, design optimization, prototyping, and SHM strategy definition (Figure 1). In the first phase (*condition assessment*), initial conditions are determined to identify climate conditions, material characteristics, available equipment, and software applications. Climate conditions, such as temperature and humidity of the environment, provide insights for designing clay mixtures and for assessing drying processes. Clay mixtures are designed by mixing clay, aggregates, binders, and water, to achieve a material that is extrudable by the equipment (i.e., clay printer). The material characteristics of the clay mixtures are determined by material testing to assess extrudability, buildability, small-scale shrinkage, and cracking behavior based on established testing methods. For each material test, four specimens are tested. Specifically, in this study, shrinkage and cracking are assessed by non-standardized testing, where customized cylindrical specimens are printed and evaluated.

In the second phase (*constraint definition*), constraints are defined by identifying and categorizing limitations based on the initial conditions, including structural, fabrication, and sensing constraints. The structural constraints are based on the flowability, strength, buildability, and shrinkage performance of the material. The fabrication constraints (e.g., layer height, built height, overhang angle, and bridging length) are determined through process parameter tests [12-15]. For each process parameter test, two specimens are tested. The sensing constraints include sensor size and sensor type restrictions, which affect design decisions in the next phase.

In the third phase (*design optimization*), design variables are identified and optimized based on the structural constraints, the fabrication constraints, and the sensing constraints. Through parametric design, infill patterns and connections are optimized for material reduction and structural integrity based on the structural constraints. The print path is then refined based on print speed and fabrication constraints, taking into account the process parameters previously defined to ensure the manufacturability of the optimized structure while considering the sensing constraints. The design process utilizes software applications for parametric design options, enabling efficient parameter adjustments without redesigning the workflow. In this study, the software application *Rhino 8* [16] is used for the parametric design, primarily motivated by the integrated visual programming tool *Grasshopper 3D*.

In the fourth phase (*prototyping*), physical prototypes are developed and evaluated to refine the design and to ensure structural integrity and manufacturability. The prototypes are fabricated to define the SHM strategy with emphasis on sensor positioning. with one prototype produced per clay mixture. The prototypes facilitate assessing changes in observable parameters (e.g., moisture content and drying direction), the respective structural behavior (e.g., shrinkage and desiccation cracking), and the related material testing (e.g., small-scale shrinkage tests).

In the fifth phase (*SHM strategy definition*), the SHM strategy is defined, based on the experimentally assessed structural behavior (e.g., shrinkage and desiccation cracking). The SHM strategy considers interactions observed between structural behavior and parametric design, when defining sensor type and sensor positions. For example, monitoring shrinkage includes selecting sensor types to observe temperature and moisture content and providing criteria for systematically determining sensor positions. The criteria determine sensor positions based on potential failure scenarios, ensuring comprehensive coverage of critical structural vulnerabilities, particularly those caused by desiccation cracks. Finally, a feedback loop facilitates adjusting the parametric design to fit the defined SHM strategy, where sensors are embedded into clay-printed prototypes to validate the SHM strategy. In the following section, the implementation of the methodology is presented.

3 EXPERIMENTAL TESTING

The methodology is implemented by experimental testing to derive the SHM strategy. The following subsections are structured in compliance with the aforementioned phases of the methodology, shown in Figure 1.

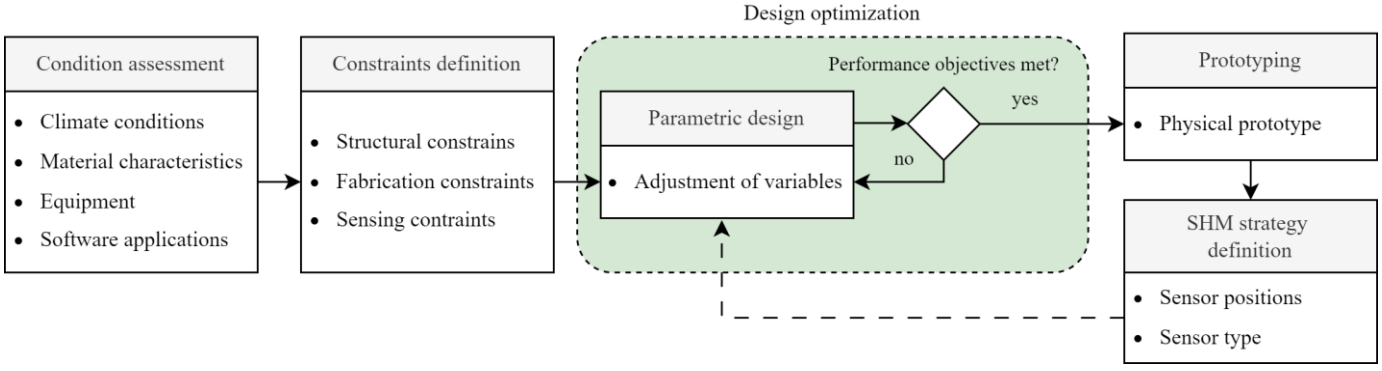

Figure 1. General workflow for determination of SHM strategies in clay printing.

DOI: 10.3217/978-3-99161-057-1-149

3.1 Condition assessment and constraints definition

The tests are conducted in a laboratory container of the Institute of Digital and Autonomous Construction. The container is maintained at a constant temperature of 23 °C. The robotic system is a 3D Potterbot Scara v4, equipped with a linear ram extruder and 3.5 l extrusion tubes that can print plastic clays. As shown in Figure 2, material tests are performed on a designated testing area, while process parameter tests are conducted on a separate levelling board. The levelling board ensures a flat printing surface and enhances adhesion due to its rough texture.

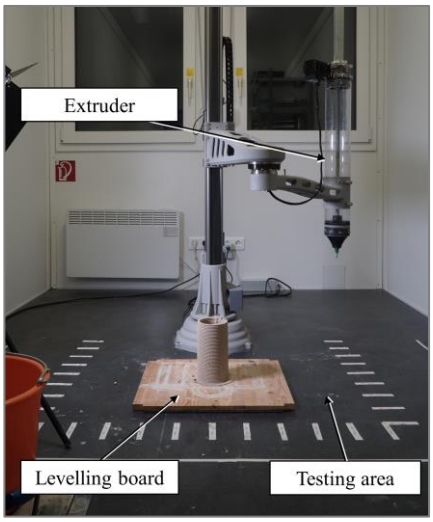

Figure 2. Experimental setup of the clay printer and print area in the laboratory container.

Clay mixtures are designed using two clay types, “clay A” representing a raw clay and “clay B” representing a milled clay. Quartz sand is added to the mixtures to increase stability and reduce shrinkage, and a starch binder is added to improve mechanical behavior. The residual moisture in the sand is below 0.3 %, with a grain size ranging from 0.062 mm to 0.3 mm. The binder, Optapix S 51, consists of modified starch with a bulk density of 0.5 kg/m^3. The physical properties and the chemical composition of clay and sand are listed in Table 1.

Table 1. Physical properties and chemical composition for clay types and sand (percentages in M-%).

	Clay A	Clay B	Quartz sand
Density [g/cm^3]	2.65	2.65	1.3 ± 0.3
Drying shrinkage [%]	4.0	6.0	-
SiO_2 [%]	75.0	71.0	92.1
Al_2O_3 [%]	19.8	24.0	2.7
TiO_2 [%]	1.4	2.0	0.0
Fe_2O_3 [%]	0.9	1.0	0.1
CaO [%]	0.2	0.0	0.9
MgO [%]	0.3	0.0	0.2
K_2O [%]	2.2	3.0	1.5
Na_2O [%]	0.1	0.0	0.2

A detailed testing workflow is created (Figure 3), comprising material composition, material parameters, and process parameters. First, material composition tests are conducted for each mixture, to determine and evaluate viable ratios of clay, sand, binder, and water. The material composition tests consist of a simple extrusion test, where the consistency and extrudability of the clay mixtures are evaluated. Results achieved from the material composition tests, 19 viable clay mixtures are obtained.

Second, the material parameters of the viable clay mixtures are evaluated, including flowability, wet strength, buildability, and shrinkage. The tests to determine the flowability, strength, and buildability consist of a cylinder drop test according to [12] and a shape retention test according to [13]. For the (non-standardized) shrinkage test, customized cylindrical specimens are printed and observed for horizontal shrinkage, vertical shrinkage, and cracking behavior. The cylindrical specimens have a diameter of 150 mm and a height of 200 mm. As a result of the material parameter evaluation, 6 viable mixtures are selected from the previous 19 mixtures previously achieved.

Third, the process parameters are determined for each mixture via extrusion line tests, failure tests, double cone tests, and bridging tests, in compliance with [14] and [15]. The process parameters are utilized to determine the fabrication constraints for designing wall components. A clay content of

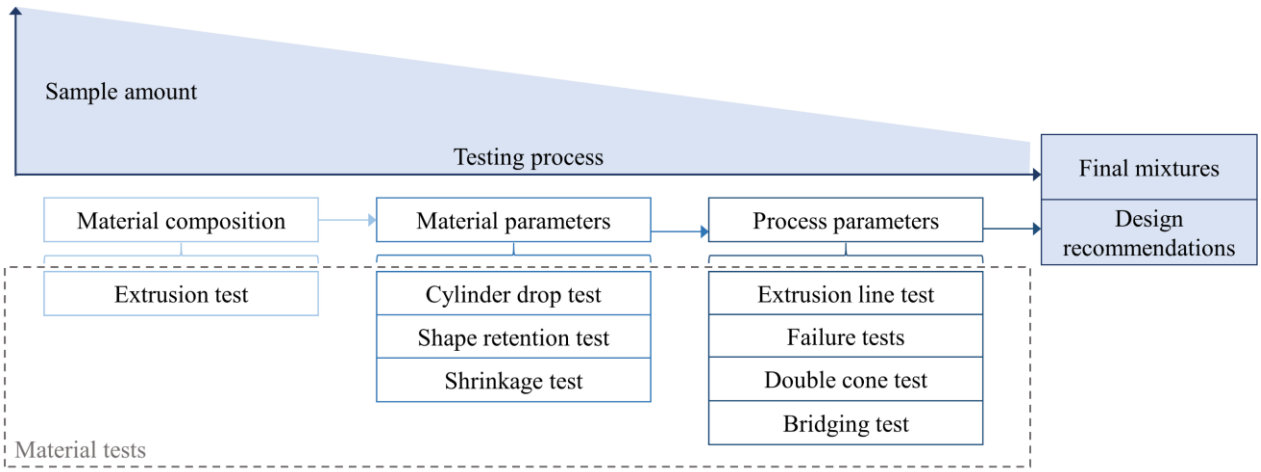

Figure 3. Material testing workflow.

DOI: 10.3217/978-3-99161-057-1-149

Table 2. Material testing clay mixture proportions.

Name	Clay [M-%]	Sand [M-%]	Water [M-%]	Binder [M-%]
A_25.0C_36.0W_1.0B	32.9	29.0	15.1	0.8
B_25.0C_38.0W_1.0B	32.6	28.6	15.6	0.8

Table 3. Process parameters defined for design considerations.

Parameter	A_25.0C_36.0W_1.0B	B_25.0C_38.0W_1.0B
Layer height for 11 mm layer width	4.5 mm	4.0 mm
Maximum build height	243 mm	356 mm
Maximum inward angle	30.0°	27.5°
Maximum outward angle	27.5°	27.5°
Bridging length, adjacent layer spacing > 0 mm	40 mm	20 mm
Bridging length, adjacent layer spacing < 0 mm	80 mm	80 mm

25 % of the dry volume is observed to offer an optimal balance between shrinkage and stability, resulting in a suitable choice for prototyping applications. Therefore, two clay mixtures *A_25.0C_36.0W_1.0B* and *B_25.0C_38.0W_1.0B* are selected for prototyping; material composition is detailed in Table 2. The corresponding process parameters are listed in Table 3.

3.2 Design optimization

The design optimization includes design variable adjustments of infill patterns, segmentation, and connection design. The infill is optimized by reducing the total material volume and print speed. Through a curved geometry, the material is reduced while retaining stability. Intersection width of adjacent curves are increased to accommodate the sensor width. The process parameters defined in the fabrication constraints regarding overhang angle and build height influence segmentation and connection design. Additional factors, including layer height, determine the toolpath configuration. Furthermore, by defining toolpaths as continuous paths, print times are reduced as retraction points and non-printing moves are minimized.

3.3 Prototyping

Two prototype specimens of a wall component, prototype A (fabricated with the mixture using clay A) and prototype B (fabricated with the mixture using clay B), are devised respectively. Buckling, overhang angles, and surface quality are visually assessed immediately after fabrication. Following the fabrication, the prototypes are evaluated during and after the drying process on shrinkage and cracking.

The prototypes are observed to be printable with no failures or significant buckling of either the contour or the infill. Observations during the drying process reveal non-uniform drying patterns in the two prototype specimens. The drying process showcases a directional gradient, characterized by drying progressing from the top to bottom and from the exterior surfaces toward the interior infill.

Moisture content assessment, conducted after a six-day drying period, reveals variations between the prototype specimens. Figure 4 shows the moisture retention behaviors of the two prototype specimens. Prototype A demonstrates faster drying rate, with faster moisture dissipation across the specimen. Conversely, prototype B exhibits a slower drying rate, as evidenced by a darker discoloration of the infill and contours, indicating retained moisture.

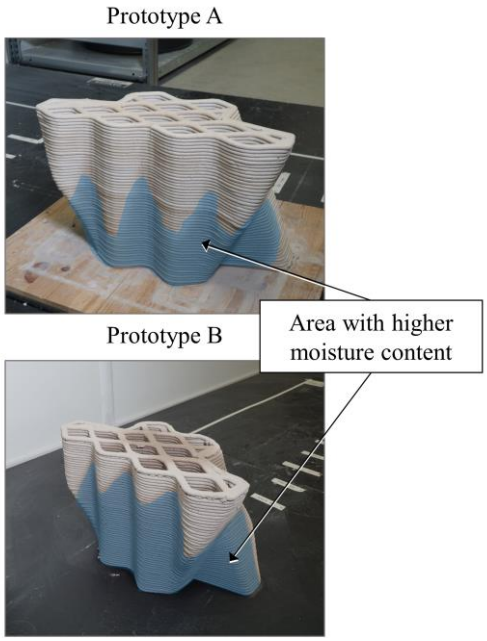

Figure 4. Prototype moisture content observed after a six-day drying period.

Desiccation cracks are documented during the drying process. On the one hand, prototype A develops multiple desiccation cracks (
Figure 5). The first cracks appear after day four, primarily centered in the midline region advancing from bottom to top, with a final length of 226 mm and width of 2 mm. Further cracks appear in the midline and front region in days six and eight and increase in length during the following days, with a final length of 223 mm and 95 mm and a final width of 1 mm, respectively. The crack at the midline region may represent a protentional weak point due to the location, length, and width of the crack. On the other hand, prototype B exhibits significantly reduced desiccation cracks with only a single crack forming after eight days at the midline region observed to advance from bottom to top. The location of the crack is similar to the position observed in the first crack of prototype

DOI: 10.3217/978-3-99161-057-1-149

A. However, the crack length and width are less severe, with a 140 mm in length and less than 1 mm in width.

Upon drying, shrinkage is evaluated by measuring the dimensions of the dry specimens and comparison with the initial dimensions. The measurements include the length on long side, length on short side, width, and height of each prototype specimen. Uneven shrinkage of the prototype is observed across the two specimens after two weeks of drying. For prototype A, a horizontal shrinkage of 5.34 % and a vertical shrinkage of 0.64 % is observed on average. Comparatively, for prototype B, a horizontal shrinkage is 6.76 % and a vertical shrinkage is 2.2 % is observed on average. The prototype A shows strong adhesion to the leveling board, resulting in reduced shrinkage at the base. In contrast, a free shrinkage at base of prototype B is noticeable due to low adhesion to the smooth bed plate. However, the prototype specimens are inaccurate for shrinkage material characterization due to the complexity of the geometry.

The difference in the shrinkage behavior of both prototypes may be attributed to the drying rate and to local errors, such as air bubbles in the extruded material, during printing. An increase in water content leads to increased shrinkage, as observed in the shrinkage evaluation, where prototype A showed less shrinkage than prototype B. Typically, increased shrinkage and faster drying processes are associated with increased desiccation cracking. However, errors during printing may cause additional cracking due to induced internal stresses, as observed by the strong adhesion to the leveling board showcased by prototype A. Special attention should be paid to the printing setup and drying rate to minimize desiccation cracking.

To define the SHM strategy, a second prototype iteration is conducted, where moisture sensors are embedded. Considering the shrinkage behavior exhibited by prototype B, the mixture using clay B is selected for the second prototype iteration (prototype B2). The prototype B2 serves to assess the effectiveness of the monitoring system and to refine the sensor positioning that will be relevant to the SHM strategy to be proposed.

3.4 Sensor integration for SHM strategy definition

As a basis to define the SHM strategy, which will be proposed in the following section, sensor integration of varying sensor types and positions is investigated. A validation test is conducted to assess the performance of resistive and capacitive moisture sensors, as well as the effect of sensor positions. Resistive and capacitive moisture sensors are typically used to measure soil moisture content using different sensing principles. Therefore, by deploying both sensor types to monitor drying processes in clay printing, the sensitivity of the sensors for detecting changes in moisture content may be compared to asses performance. As shown in Figure 6, two sensor systems are used to monitor prototype B2,

(i) sensor system I, a ***commercial sensor system*** consisting of a resistive moisture sensor typically used for discrete soil monitoring, and
(ii) sensor system II, a ***custom-made SHM system*** consisting of a moisture sensor node (containing three capacitive moisture sensors) and an environmental sensor node for continuous monitoring of clay moisture content and the surrounding environment.

The resistive and capacitive moisture sensors are positioned at different embedment depths and distributed on the exterior and interior surfaces of prototype B2 to monitor the drying process following the observed drying gradient during the prototyping phase.

On the one hand, sensor system I is designed to measure soil moisture by outputting a value of resistance between the two probes. On the other hand, sensor system II is designed for recording real-time data of the prototype moisture content and the environmental conditions in the laboratory. The moisture sensor node of sensor system II comprises the three embedded capacitive moisture sensors v2.0 that are connected via cables to an Arduino ESP32 microcontroller to record moisture content by detecting changes in capacitance. The capacitive

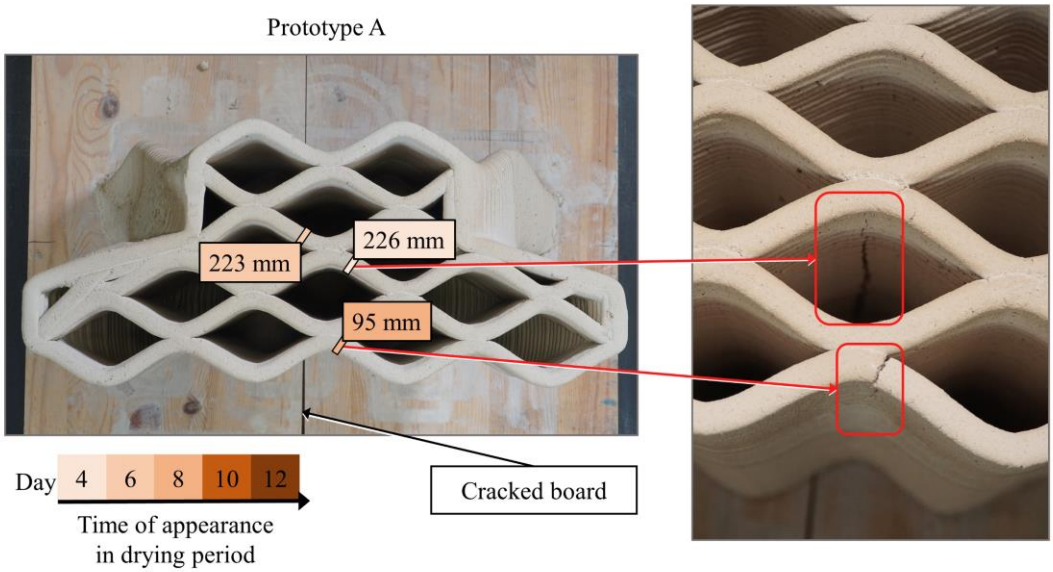

Figure 5. Desiccation cracks in prototype A.

DOI: 10.3217/978-3-99161-057-1-149

sensors are embedded at a depth of two-thirds of the sensor length. The environmental sensor node consists of an Si7021 temperature and humidity sensor connected to a microcontroller for recording environmental conditions. The data recorded by both sensor nodes is transmitted via a cable connection to a base station (i.e. Raspberry Pi microcomputer) that serves as a datalogger for data management and storage. It should be noted that the capacitive moisture sensors are calibrated in both dry and fresh clay conditions using the pre-calibrated sensor system I as benchmark.

The positioning of the embedded moisture sensors of both sensor systems is determined by the respective geometric constraints. The resistive sensor of sensor system I consists of two probes, each 180 mm in length and spaced 30 mm apart. The capacitive soil moisture sensors of sensor system II measure 98 mm in length, 23 mm in width, and 4 mm in thickness. Considering a layer width of 11 mm, the sensors are embedded vertically at overlying points within the structure to minimize any impact on structural stability. Furthermore, to evaluate the effect of the sensor positions, three embedment depths are defined (Figure 7). The capacitive sensors of the moisture sensor node of sensor system II are positioned following the printing process, where Sensor 1 (printing time t = 60 min) and Sensor 2 (t = 112 min) are fully embedded during printing, while Sensor 3 (t = 147 min) is partially embedded. The probes of the resistive sensor (Sensor 4) of sensor system I are also partially embedded at t = 147 min. Due to the length of the probes of Sensor 4, Sensor 2, and Sensor 4 record moisture content at approximately the same height. A special consideration is given to the capacitive sensors, where a permeable membrane is wrapped around the sensing elements of the sensors that are in contact with clay to facilitate local moisture evaporation. Sensor cables are routed through the infill gaps, which serve as cable channels, and are connected to the microcontroller after the printing process.

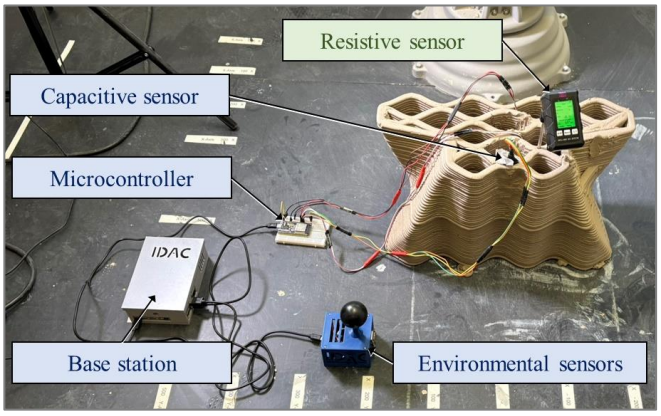

Figure 6. Components of sensor system I (blue) and sensor system II (green).

Prototype B2 is monitored over 10 days, and the moisture content is recorded continuously by sensor system II, while sensor system I is read manually three times daily. No structural instabilities or sensor-induced cracking are observed during this period.

The environmental data (Figure 8) shows humidity levels ranging from 15 % to 40 % and temperatures between 18.1 °C and 23.8 °C. The declining moisture content in the structure (Figure 9) corresponds with these environmental changes. Capacitive sensors (Sensors 1-3) exhibit a stabilization phase of approximately 25 h, due to the membrane barrier. The fully embedded sensors (Sensor 1 and 2) reveal nearly identical trends, while partially embedded sensor 3 shows higher initial moisture levels during the first 160 h.

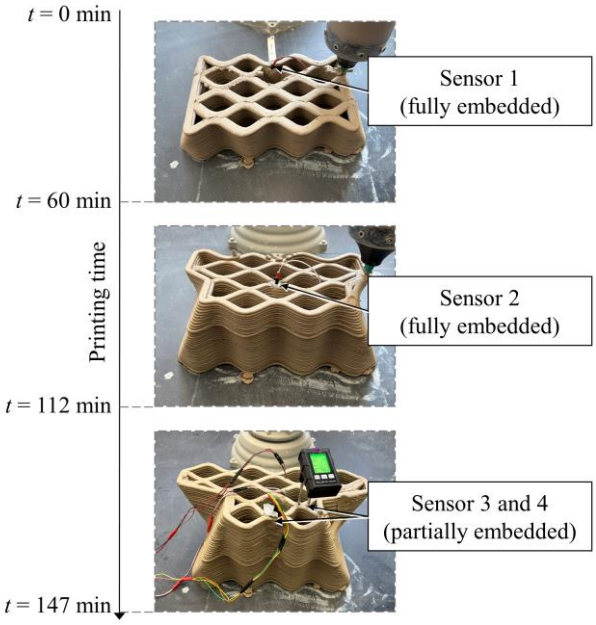

Figure 7. Embedded sensor integration during the printing process.

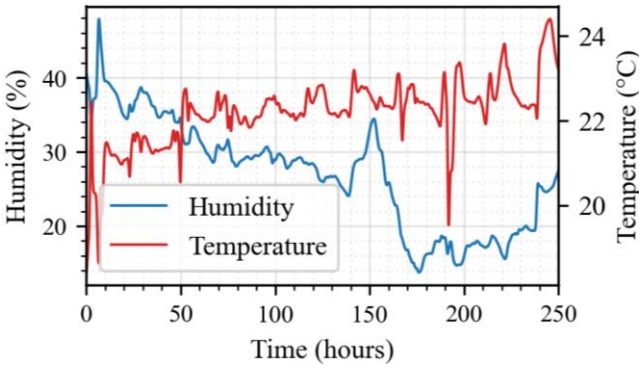

Figure 8. Environmental sensor readings.

Furthermore, as observed from Figure 9, the resistive sensor (Sensor 4) showcases higher values of moisture content compared to the capacitive sensors in the first 195 h of measurement, followed by a sharp drop of moisture content. Although a similar moisture content trend was expected between Sensor 2 and Sensor 4, the values observed for Sensor 4 indicate that the resistance-based sensing principle is not as sensitive to the change of moisture content compared to capacitive-based sensing principle. By observing the cumulative soil moisture loss over time (Figure 10), a total moisture loss ranging from 43 % to 48 % is observed. The measured cumulative moisture loss from Sensor 1 and Sensor 3 are comparable, while Sensor 2 deviates slightly in an acceptable range. In contrast, Sensor 4 deviates significantly, further indicating limited accuracy and responsiveness.

DOI: 10.3217/978-3-99161-057-1-149

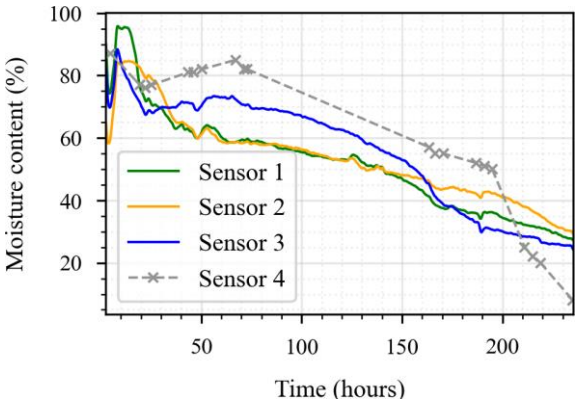

Figure 9. Moisture sensor readings (sensors are calibrated for dry mixture = 0%, wet mixture = 100%).

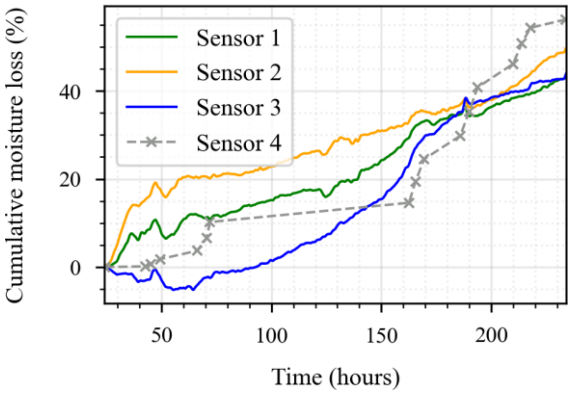

Figure 10. Cumulative moisture loss over time (starting at t = 25 h).

4 DISCUSSION AND SHM STRATEGY DEFINITION

In this section, the results of the sensor integration are discussed as a basis for the SHM strategy definition, subsequently proposed in this section.

4.1 General discussion of the results

The moisture sensors have demonstrated varying accuracy. Fully embedded sensors have shown nearly identical values, while the partially embedded sensors have tended to record higher moisture levels. Following initial surface water loss, the sensor readings have aligned with the visual observations, reflecting the drying conditions of prototype B2. The absolute moisture readings have been inconsistent between sensor types and absolute measurement results have not been quantified by means of measuring the component weight over time. However, the recorded trends of capacitive soil moisture sensors have correlated with the expected structural performance and visual assessments, suggesting the suitability of capacitive measuring for relative monitoring. The permeable membranes have delayed the moisture penetration causing additional time for sensor stabilization. Capacitive changes have been detected by the embedded sensors with varying accuracy, depending on sensor type and position; however, measurements of capacitive moisture sensors have successfully captured the drying gradient within prototype B2. The environmental conditions have significantly influenced the drying process, with accelerated moisture loss observed under lower humidity and elevated temperature.

Overall, the findings underline the applicability of moisture sensors for monitoring moisture loss in additively manufactured clay structures and form the basis for developing a tailored SHM strategy.

4.2 SHM strategy

Defining the SHM strategy for clay-printed structures requires careful selection and placement of sensors tailored to specific monitoring objectives. Clay moisture and environmental conditions must be assessed to evaluate structural integrity, while visual inspections aid in optimizing sensor placement. Different sensor types serve distinct monitoring purposes: Moisture sensors enable tracking of drying behavior, whereas stability sensors, such as strain gauges, allow detecting buckling and shrinkage, and provide long-term data on internal stress states. In this study, both capacitive and resistive moisture sensors have proven capable of capturing drying behavior in the conducted experiments. However, resistive sensors are more susceptible to corrosion and exhibit a high sensitivity to increased ion concentrations, such as salt, which are prominent in clay. Salts decrease the resistance between sensor nodes and, therefore, the sensors read comparatively increased moisture values. Capacitive sensors, by contrast, have shown greater reliability and resolution, rendering capacitive sensors a more promising choice for continued application in SHM strategies. Sensor placement should follow the observed (or expected) drying gradients, to enable accurate assessment of moisture migration and identification of zones prone to cracking. Due to the evolving geometry and temporal variability inherent to additive manufacturing, a fundamental decision must be made regarding the embedding time, i.e. whether the sensors are integrated during or after the printing process. Embedded wired sensors introduce challenges, including the risk of crack formation at cable transition points caused by clay shrinkage. The cracks may compromise structural stability or facilitate moisture ingress. Although infill gaps can serve as routing channels for sensor cabling, the geometrical complexity of 3D-printed components poses significant limitations for scaling wired sensor networks.

Therefore, wireless monitoring solutions are a prerequisite for scalable SHM in clay-printed structures. However, the physical properties of clay pose substantial challenges for embedded wireless communication. The high dielectric constant and moisture retention of clay lead to significant attenuation of high-frequency radio waves, thereby impairing signal transmission. Elevated moisture content intensifies the effect by increasing material conductivity and absorbing radio frequency (RF) energy, causing reduced transmission efficiency. Additionally, multipath interference, owing to RF signal reflection and scattering within the heterogeneous internal structure of clay, may lead to signal distortion and data loss. To ensure reliable wireless sensing, careful selection of operating frequencies and the implementation of adaptive communication protocols are required, to account for the variable electromagnetic properties of clay throughout the drying process. Furthermore, current technological limitations constrain the deployment of SHM systems: Low-cost capacitive sensors often lack the required accuracy, standard resistive sensors remain prone to corrosion, and both exhibit

DOI: 10.3217/978-3-99161-057-1-149

limited sensitivity to gradual moisture changes. When implementing SHM strategies for clay-printed structures, attention must be paid to the aforementioned constraints by enhancing sensor robustness, measurement precision, and wireless operability. Particular attention should as well be given to the development of embedded, miniaturized wireless sensors capable of long-term, real-time data acquisition in the challenging environment of clay-printed structures.

5 SUMMARY AND CONCLUSIONS

With the increased attention on clay printing in research and practice, SHM strategies need to be tailored to fit clay-printing technologies. In this study, an SHM strategy has been proposed, and the structural properties of clay-printed structures, including buckling, shrinkage, and load-bearing capacity, have been experimentally determined. Prototyping and sensor placement validation have demonstrated the feasibility of constructing structurally stable clay-printed structures and provided key insights into material behavior (i.e., shrinkage) for deriving sensor positioning strategies.

The methodology proposed in this study has provided a structured approach to understanding clay as a 3DP material, incorporating both material characterization and an SHM strategy. The experimental results have demonstrated that effective sensor placement can be obtained through systematic analysis of material behavior, particularly focusing on drying patterns and potential fault locations. Moreover, the study has addressed relationships between small-scale laboratory tests and larger prototypes, establishing crucial scalability considerations for SHM sensor networks of large-scale structures. In summary, the findings contribute to advancing the field of sustainable construction by demonstrating the viability of clay printing based on a sound SHM strategy. Future research may include quantifying sensor results in respect to shrinkage and extending the SHM strategy from cable-based to wireless systems.

ACKNOWLEDGMENTS

Financial support provided by the German Research Foundation (DFG) through grants SM 281/22-1 and SM 281/31-1 as well as by Hamburg University of Technology via the I³ program under the junior project *Digitalization of Earth Printing to Advance Climate-Informed Engineering* is gratefully acknowledged. The authors express their gratitude to Goerg & Schneider GmbH & Co. KG for supplying the clay material. The opinions, findings, conclusions, and recommendations presented in this paper are solely those of the authors and do not necessarily reflect the views of the sponsoring organizations.

REFERENCES

[1] Ponis, S., Aretoulaki, E., Maroutas, T. N., Plakas, G., and Dimogiorgi, K., 2021. A systematic literature review on additive manufacturing in the context of circular economy. Sustainability, 13(11), 6007.

[2] Peralta, P. & Smarsly, K., 2022. Requirements analysis of additive manufacturing for concrete printing – A systematic review. In: Proceedings of the 39th International Symposium on Automation and Robotics in Construction (ISARC). Bogota, Colombia, 07/12/2022.

[3] Smarsly, K., Peralta, P., Luckey, D., Heine, S. & Ludwig, H.-M., 2020. BIM-based concrete printing. In: Proceedings of the International ICCCBE and CIB W78 Joint Conference on Computing in Civil and Building Engineering. Sao Paolo, Brazil, 08/18/2020.

[4] Peralta, P., Ahmad, M. E. & Smarsly, K., 2023. Printing information modeling (PIM) for additive manufacturing of concrete structures. Applied Sciences, 13(23), 12664.

[5] Hong, C., Zhang, Y. & Borana, L., 2022. Performance investigation of 3D printed clay soil using fiber Bragg grating technology. Acta Geotechnica, 17(2), pp. 453-462.

[6] Peralta, P., Heine, S., Ludwig, H.-M. & Smarsly, K., 2020. A BIM-based approach towards additive manufacturing of concrete structures. In: Proceedings of the 27th International Workshop on Intelligent Computing in Engineering. Berlin, Germany, 07/01/2020.

[7] Ma, G., Li, Y., Wang, L., Zhang, J. & Li, L., 2020. Real-time quantification of fresh and hardened mechanical property for 3D printing material by intellectualization with piezoelectric transducers. Construction and Building Materials, 241(2020), 117982.

[8] Tanapornraweekit, G., Jiramarootapong, P., Paudel, S., Tangtermsirikul, S. & Snguanyat, C., 2022. Experimental and numerical investigation of 3D-printed mortar walls under uniform axial compression. Construction and Building Materials, 360(2022), 129552.

[9] Hassani, S. & Deckermann, U., 2023. A systematic review of advanced sensor technologies for non-destructive testing and structural health monitoring. Sensors, 23(4), 2204.

[10] Panda, B. & Tan, M.J., 2019. Rheological behavior of high-volume fly ash mixtures containing micro silica for digital construction application. Materials Letters, 237(2019), pp. 348-351.

[11] Tang, C.-S., Shi, B., Liu, C., Suo, W.-B. & Gao, L., 2011. Experimental characterization of shrinkage and desiccation cracking in thin clay layer. Applied Clay Science, 52(1–2), pp. 69-77.

[12] Perrot, A., Rangeard, D. & Lecompte, T., 2018. Field-oriented tests to evaluate the workability of cob and adobe. Materials and Structures, 51(2018), 54.

[13] Kazemian, A., Yuan, X., Cochran, E. & Khoshnevis, B., 2017. Cementitious materials for construction-scale 3D printing: Laboratory testing of fresh printing mixture. Construction and Building Materials, 145(2017), pp. 639-647.

[14] Gomaa, M., Jabi, W., Veliz Reyes, A. & Soebarto, V., 2021. 3D printing system for earth-based construction: Case study of cob. Automation in Construction, 124(2021), 103577.

[15] Curth, A., Pearl, N., Castro-Salazar, A., Mueller, C. & Sass, L., 2024. 3D printing earth: Local, circular material processing, fabrication methods, and life cycle assessment. Construction and Building Materials, 421(2024), 135714.

[16] Robert McNeel & Associates, "Rhinoceros 3D," www.rhino3d.com.